Complement Activation on B Lymphocytes Opsonized with Rituximab or Ofatumumab Produces Substantial Changes in Membrane Structure Preceding Cell Lysis[1]

Paul V. Beum,* Margaret A. Lindorfer,* Frank Beurskens,[†] P. Todd Stukenberg,* Henk M. Lokhorst,[‡] Andrew W. Pawluczkowycz,* Paul W. H. I. Parren,[†] Jan G. J. van de Winkel,[†§] and Ronald P. Taylor[2]*

Binding of the CD20 mAb rituximab (RTX) to B lymphocytes in normal human serum (NHS) activates complement (C) and promotes C3b deposition on or in close proximity to cell-bound RTX. Based on spinning disk confocal microscopy analyses, we report the first real-time visualization of C3b deposition and C-mediated killing of RTX-opsonized B cells. C activation by RTX-opsonized Daudi B cells induces rapid membrane blebbing and generation of long, thin structures protruding from cell surfaces, which we call streamers. Ofatumumab, a unique mAb that targets a distinct binding site (the small loop epitope) of the CD20 Ag, induces more rapid killing and streaming on Daudi cells than RTX. In contrast to RTX, ofatumumab promotes streamer formation and killing of ARH77 cells and primary B cells from patients with chronic lymphocytic leukemia. Generation of streamers requires C activation; no streaming occurs in media, NHS-EDTA, or in sera depleted of C5 or C9. Streamers can be visualized in bright field by phase imaging, and fluorescence-staining patterns indicate they contain membrane lipids and polymerized actin. Streaming also occurs if cells are reacted in medium with bee venom melittin, which penetrates cells and forms membrane pores in a manner similar to the membrane-attack complex of C. Structures similar to streamers are demonstrable when Ab-opsonized sheep erythrocytes (non-nucleated cells) are reacted with NHS. Taken together, our findings indicate that the membrane-attack complex is a key mediator of streaming. Streamer formation may, thus, represent a membrane structural change that can occur shortly before complement-induced cell death. *The Journal of Immunology,* 2008, 181: 822–832.

R ituximab (RTX)[3] is a chimeric human-mouse mAb specific for CD20 currently used in the treatment of B cell lymphomas and rheumatoid arthritis (1–8). The mechanism of action of RTX remains to be fully elucidated, but both Ab-dependent cell-mediated cytotoxicity and complement (C)-mediated cytotoxicity appear to play roles in its therapeutic action (9–27). Our studies, as well as those of others, have revealed that binding of RTX to CD20$^+$ cells activates C both in vitro and in vivo (10, 19, 28). As a consequence of C activation, large amounts of C3b and its breakdown products are covalently deposited on the cells, in close proximity to bound RTX (28, 29). This reaction is then followed downstream by assembly of membrane attack complexes (MAC) of C, pore-forming cytotoxic agents that penetrate the cell and induce lysis.

To study the dynamics of these reactions in real time, we have used spinning disk confocal microscopy (SDCM) (30) to examine C3b deposition and cell killing mediated by both RTX and ofatumumab (OFA) (31–33). OFA is a unique mAb that targets a distinct binding site (the small loop epitope) of the CD20 Ag. OFA, upon binding to B cells, is able to promote more effective complement activation and cell killing than RTX. SDCM is much less damaging to live cells than traditional scanning confocal microscopy by virtue of the laser light being focused on a given point for shorter times and, thus, allows for analysis of processes in live cells (30). We have obtained real-time movies showing deposition of C3b fragments on, as well as killing of, B cells opsonized with CD20 mAbs RTX or OFA. We studied the dynamics of C3b deposition based on use of mAb 3E7, which binds with high avidity to C3b deposited on cells even in normal human serum (NHS), when large amounts of competing C3b activation fragments are produced in the surrounding milieu (19).

Reaction of mAb-opsonized B cells with C rapidly induces dramatic morphologic changes in the cells, including blebbing and the generation of long thin structures we term streamers, which extend from the cell membrane. Several experiments indicate that blebbing and streamer formation are likely a direct result of attack on the cells by the MAC of C. These analyses demonstrate that there are substantial differences between RTX and OFA, as observed in movies generated for periods of only 2–15 min, in which OFA is considerably more efficient with respect to the dynamics and efficacy of C3b deposition, streamer formation, and cell killing.

Materials and Methods

Cell culture and reagents

CD20$^+$ Daudi and ARH77 cells were obtained from American Type Culture Collection and cultured as previously described (19, 34). Blood was obtained from patients with chronic lymphocytic leukemia (CLL) and from normal individuals and mononuclear cells were isolated as described previously (34), washed, and reconstituted in RPMI 1640 media. B cells from normal blood donors were isolated from mononuclear cell preparations using a B cell isolation kit (negative selection) from Miltenyi Biotech (34). University of Virginia Institutional Review Board approved all protocols. RTX was obtained at the University of Virginia hospital pharmacy, and OFA was provided by Genmab. Monoclonal Ab 3E7, specific for C3b/iC3b, has been described (19). RTX, OFA, and mAb 3E7 were labeled with Alexa (Al) 488, Al546, or Al647 (Invitrogen), according to the manufacturer's instructions. In comparison experiments of OFA with RTX, the fluorophore/protein ratios (2/1) of the two mAbs were carefully matched. F(ab')$_2$ of RTX were generated using the ImmunoPure F(ab')$_2$ preparation kit from Pierce following the manufacturer's directions. Sheep erythrocytes were obtained from Lampire. Al488 phalloidin was purchased from Invitrogen. Bee venom melittin, PKH 26 red fluorescent membrane dye, anti-sheep RBC stroma (hemolysin), cytochalasin D, nocodazole, and sodium azide were from Sigma-Aldrich. C5-depleted serum, C9-depleted serum, and purified C5 and C9 were obtained from Complement Technology. Viability dye 7-aminoactinomycin D (7-AAD) was from BD Pharmingen. Normal human serum (NHS) consisted of pooled sera obtained from healthy donors.

OFA- and RTX-mediated killing of Daudi and ARH77 cells in the presence of NHS was measured following our published procedures (28, 34); TO-PRO-3 (Invitrogen) was used to differentiate live from dead cells.

Opsonization of cells and preparation for analysis

The B cells were first opsonized with the CD20 mAbs as follows: 5×10^6 Daudi or ARH77 cells in 0.5 ml RPMI 1640 were incubated for 15 min at 37°C with gentle shaking, with saturating concentrations (10 μg/ml) of Al488 RTX, Al647 RTX, Al488 OFA, or Al647 OFA (31, 34, 35), and then washed three times with BSA/PBS, and resuspended in a final volume of 50 μl RPMI 1640. A 5 μl aliquot of the opsonized cells was mixed with 5 μl of test mixture (containing NHS) on ice or at room temperature, giving a final density of 5×10^7 cells/ml and a final NHS concentration of either 25 or 50%, and 4 μl of the mixture was immediately placed on a slide with a cover slip and analyzed by SDCM (see below) or by fluorescence microscopy (FM). The total elapsed time from combination of the cells with the test mixture to the start of the movies was always <2 min. The exact composition of the test mixture varied depending on the specific experiment and is specified in the figure legends. In many of these studies, we made use of mAb 3E7 because this mAb recognizes and binds to a neoepitope on C3b when it is deposited on cells and only weakly binds to native C3 or activated C3b that reacts with water (19). When present, Al647 mAb 3E7, Al546 mAb 3E7, or Al488 mAb 3E7 was included in the mixture at 20 μg/ml, thus, making it possible to visualize and follow C3b deposition in real time.

In experiments using sheep E, the E were first washed extensively with gelatin veronal buffer (GVB) containing 0.01 M EDTA (GVBE), and then reacted with reconstituted anti-sheep E stroma (hemolysin) for 15 min at 37°C (28, 36). The cells (sheep erythrocytes opsonized with complement-fixing Abs, EA) were washed several times with GVBE and then labeled with 2 μM PKH 26 (37) following the manufacturer's instructions, and finally washed and resuspended in GVB supplemented with 0.15 mM Ca^{2+} and 0.5 mM Mg^{2+}. Aliquots of the PKH 26-labeled EA were then mixed with varying concentrations of NHS, and either analyzed immediately by SDCM or incubated for 2–20 min at 37°C followed by FM analysis.

SDCM and FM

For SDCM analysis, the slide was placed on a stage prewarmed to 37°C. SDCM collects images generated by the laser illuminating the sample at a single Z position at up to three wavelengths. An image is captured at a given Z position at each wavelength before the next Z position is illuminated. All the Z section images were combined into a single Z stack for each time point. The movies and still images in this report were produced using this Z stack mode. Additionally, images collected by the microscope at different wavelengths are stored in separate files on the computer, so that movies can be viewed at each of the selected wavelengths separately, or the movies at the different wavelengths can be superimposed to form a composite, or merged, movie.

Confocal images were obtained with a Zeiss Axiovert 200 inverted microscope using a ×40 or ×63 objective under oil. The microscope is linked to a Yokogawa spinning disk confocal unit (CSU21) and a krypton/argon air-cooled excitation laser. Images were collected and visualized using Ultraview RS software (PerkinElmer). Z stacks of fluorescent images were collected in real time over a period of 2–15 min. All time periods specified in the figures refer to the times after the movie was started, and do not include the ~2 min that elapsed between mixing of cells with the test mixture and the start of the movie. The resulting movies were converted to Quicktime format using the Ultraview RS software, and individual still images were captured from the movies using Adobe Photoshop. Each movie and figure is representative of at least four replicate experiments. There was some variability in the percentage of Daudi cells with streamers for experiments conducted on different days and under different conditions. The cells were scored for streamers and representative results, based on multiple independent experiments, were used to define the following scoring system, with respect to the percentage of cells with streamers: 0, no streamers detectable; 1, 2–20%; 2, 20–40%; 3, 40–60%; 4, 60–80%; and 5, 80–100%.

Most experiments with CLL cells were based on analyses of replicate slides that were examined by FM after brief incubations at 37°C. The percentage of cells with streamers or blebs was estimated by counting cells (~200) in multiple fields. In some experiments, CLL cells were incubated simultaneously with either OFA or with RTX, and with NHS and with mAb 3E7, instead of opsonizing first with OFA/RTX, washing, and then reacting with NHS and mAb 3E7. CD20 levels on CLL cells were determined by flow cytometry, converted to molecules of equivalent soluble fluorochrome, and compared with levels on Daudi cells (38). C-dependent cytotoxicity (CDC) of CLL cells reacted with OFA or with RTX was measured after incubating the cells with mAbs in 50% NHS for 30 min at 37°C, with readouts based on staining with TO-PRO-3 (19, 28, 34).

In experiments where the cells were analyzed by FM, samples were examined under oil at high magnification (×100) using a BX40 fluorescent microscope (Olympus). Images were captured with a digital camera and visualized with Magnafire analysis software (28).

Results

Activation of C on cells opsonized with CD20 mAbs promotes rapid deposition of C3b, followed by both blebbing and streaming

Daudi B cells were opsonized with excess Al488 RTX and, after three washes, they were reacted with NHS (final concentration of 50%) containing Al647 mAb 3E7, and then real-time changes in the fluorescent signals associated with the Al488 RTX and Al647 mAb 3E7 probes were examined by SDCM. The photomicrographs in Fig. 1, A–C, show three time points from the movies collected after excitation at either 488 or 647 nm and the merged images, respectively. The time zero points (start of the movie), obtained <2 min after the prepared cells were placed on a microscope slide and transferred to the heated stage, clearly demonstrate that large amounts of Al488 RTX were indeed bound to the cells (Fig. 1A). Initially less C3b was bound, as manifested by the weaker signal in the 647 nm image, which represents binding by anti-C3b/iC3b mAb 3E7 (Fig. 1B). The movies (supplemental movies 1–3)[4] and images (Fig. 1, A–C) indicate that during the period that the cells are incubated at 37°C, several processes occur: large amounts of C3b are deposited on the cells and they undergo substantial blebbing, soon followed by generation of streamers, long thin structures which appear to grow outward away from the plasma membrane. The streamers clearly contain both Al488 RTX and Al647 mAb 3E7; based on the specificity of mAb 3E7, C3b/iC3b must be present on the streamers. As is evident both in the movies and in the images, the accumulation of C3b/iC3b on the cells is rapid, and there is a moderate degree of colocalization of the green Al488 RTX with the red Al647 mAb 3E7, as shown by the yellow-orange colors in the merged images in Fig. 1C. This finding indicates that much of the C3b/iC3b must be deposited in close proximity to cell-bound RTX, in agreement with our previous observations made using more conventional

---

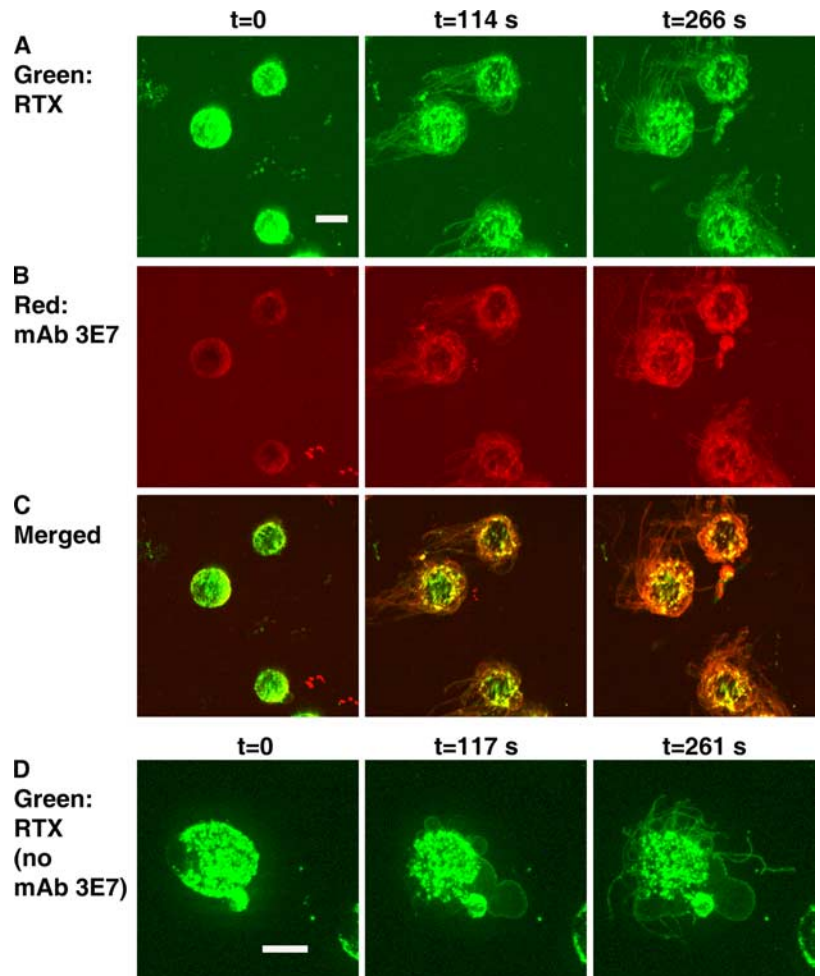[4] The online version of this article contains supplemental material.

FIGURE 1. Binding of RTX to Daudi cells in NHS induces blebbing and streaming. *A–C*, images obtained at three different times for Daudi cells reacted with Al488 RTX, Al647 mAb 3E7, and NHS. *A*, The 488 nm images show green RTX. *B*, The 647 nm images show red mAb 3E7. *C*, Merged images. Note that overlap of red and green produces orange or yellow. Also, see supplemental movies 1–3. *D*, Blebbing and streamers are generated in the absence of mAb 3E7. Daudi cells were opsonized with Al488 RTX and then reacted with NHS. Images for 488 nm are displayed at three time points. The calibration bar in this and the following figures denotes 5 microns. The magnification in *A–C* was ×40, but, in Fig. 1*D* and all other figures derived from SDCM images, ×63 magnification was used. In this figure and the other figures, additional pertinent information is enclosed in parentheses in the figures.

opsonization and probing schemes (28, 29). Production of streamers does not require and is not induced by the action of mAb 3E7; movies taken of Al488 RTX-opsonized and washed Daudi cells in the presence of NHS without mAb 3E7 also show streamers, as seen in Fig. 1*D*.

Streaming was also evident when RTX-opsonized Raji cells were incubated with NHS and mAb 3E7 (not shown), but quite rarely did we observe streaming for comparably treated ARH77 cells. ARH77 cells are quite resistant to C-mediated killing promoted by RTX (19, 31); however, the new CD20 mAb OFA activates C much more effectively than RTX and has been reported to kill ARH77 cells in the presence of NHS (31). Therefore, we examined the potential of this mAb to induce streamer formation. The SDCM movie in supplement 4 and images in Fig. 2*A* indicate that binding of OFA to Daudi cells does indeed lead to generation of streamers when the opsonized cells are incubated with NHS and mAb 3E7. Unlike RTX, however, OFA is able to robustly induce streaming in ARH77 cells (Fig. 2, *B* and *C*), which is consistent with much more effective killing of ARH77 cells by OFA. In contrast, representative images of Al488 RTX-opsonized ARH77 cells reacted with NHS in the presence of Al647 mAb 3E7 indicate that although binding of RTX to these cells is easily demonstrable, streaming is not seen and the level of C3b deposition is quite variable and often weaker than that induced by OFA (Fig. 2, *D* and *E*). Finally, we were able to positively identify Al647 OFA in the streamers when Daudi cells were reacted with Al647 OFA and NHS in the absence of mAb 3E7 (Fig. 2*F*).

The complete C pathway appears to be required for both blebbing and streaming

To further investigate the role of C in the formation of streamers, we incubated Al488 OFA-opsonized Daudi cells with Al647 mAb 3E7 and NHS to which EDTA had been added to chelate Mg^{2+} and Ca^{2+} ions and, thus, block C activation. The images in Fig. 3*A* are taken from the resulting SDCM movie of the merged 488 and 647 nm movies. The green appearance of the cells shows that Al488 OFA stably binds to the cells in NHS-EDTA. The lack of red staining of the cells by Al647 mAb 3E7 confirms that C activation and C3b deposition were inhibited, and no blebbing or streamers were detectable over the length of the movie (10 min). Similar results were obtained when cells were opsonized with either CD20 mAb followed by incubation in media alone or in heat-inactivated NHS with mAb 3E7 (not shown); that is, neither C3b deposition nor blebbing nor streaming were evident, providing additional evidence that these reactions all require C activation. We next reacted Al488 RTX-opsonized Daudi cells with C5-depleted NHS in the presence of Al546 mAb 3E7. A representative image taken from the 568 nm SDCM movie (Fig. 3*B*) shows binding of Al546 mAb 3E7 (and, thus, C3b) to the cell surface. This result is quite reasonable, as the C pathway is intact to the C3 activation step in C5-deficient serum. Fig. 3*B* also shows that no streamers are generated in C5-deficient serum, but reconstitution of the entire C pathway by addition of purified C5 restores blebbing and streaming, as seen in the 568 nm image in Fig. 3*C*. A similar
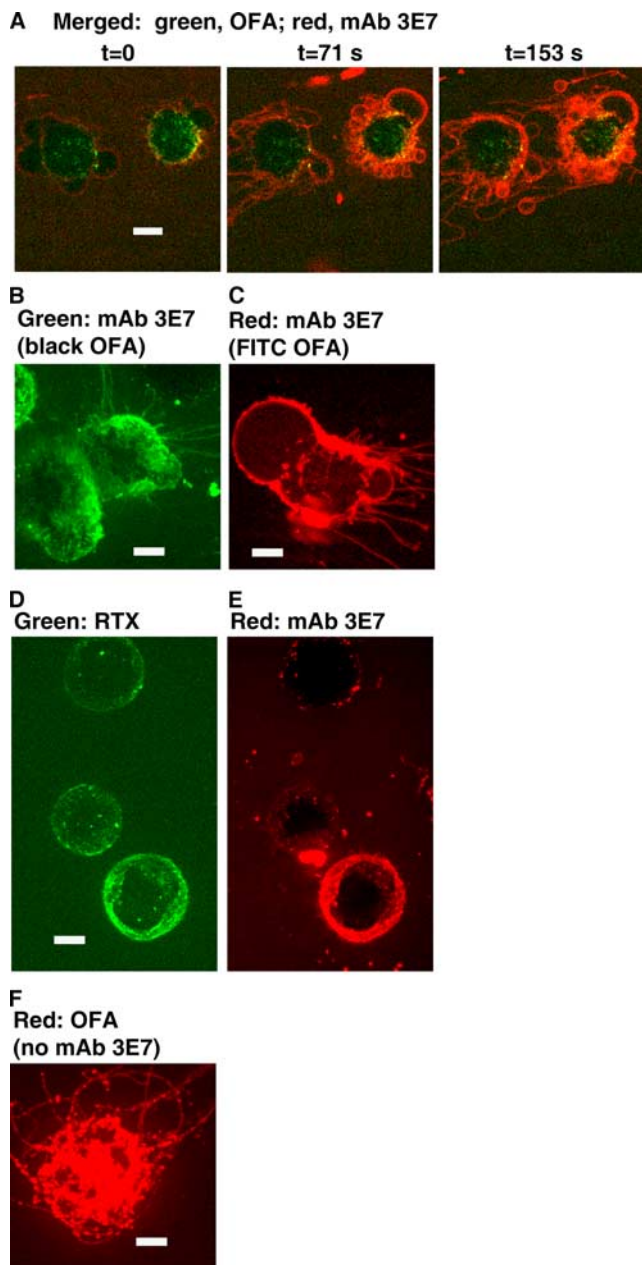
FIGURE 2. Binding of OFA to Daudi cells and ARH77 cells, followed by reaction with NHS, produces blebbing and streamers. *A*, Daudi cells were opsonized with Al488 OFA, and then reacted with NHS and Al647 mAb 3E7; merged 488 nm/647 nm images at the indicated times. Also, see supplemental movie 4. *B*, ARH77 cells were opsonized with OFA, and then reacted with NHS and Al488 mAb 3E7; 488 nm image shows mAb 3E7. *C*, ARH77 cells were opsonized with FITC OFA, and then reacted with NHS and Al647 mAb 3E7; 647 nm image shows mAb 3E7. *D* and *E*, ARH77 cells were opsonized with Al488 RTX, and then reacted with NHS and Al647 mAb 3E7; 488 nm image (*D*) shows RTX and 647 nm image (*E*) shows mAb 3E7. *F*, Blebbing and streamers are generated in the absence of mAb 3E7. Daudi cells were opsonized with Al647 OFA and then reacted with NHS. The 647 nm image is displayed.

FIGURE 3. Neither blebbing nor streamers are observed if C activation is blocked by addition of EDTA to NHS, and in C5-deficient serum and in C9-deficient serum, C3b deposition is observed, but blebbing is rarely seen and streaming is abrogated unless purified C5 and C9, respectively, are provided. *A*, Daudi cells were opsonized with Al488 OFA and then reacted with NHS-EDTA and Al647 mAb 3E7; merged 488 nm/647 nm images are shown at the indicated times. *B*, Daudi cells were opsonized with Al488 RTX and then reacted with C5-deficient NHS and Al546 mAb 3E7. *C*, C5 (80 μg/ml final concentration) was added back to the cells treated as in *B*. *D*, Daudi cells were opsonized with Al488 OFA and then reacted with C9-deficient NHS and Al647 mAb 3E7. *E*, C9 (60 μg/ml final concentration) was added back to the cells treated as in *D*. *B* and *C*, The 568 nm image shows Al546 mAb 3E7. *D* and *E*, The 647 nm image shows Al647 mAb 3E7.

experiment with OFA-opsonized Daudi cells, based on adding C9 back to C9-deficient serum (Fig. 3, *D* and *E*) provides additional evidence that the entire C pathway including the MAC is required to generate streamers (Table I). Finally, streamers and blebbing are also observed when citrated plasma is used as a complement source (Table I).
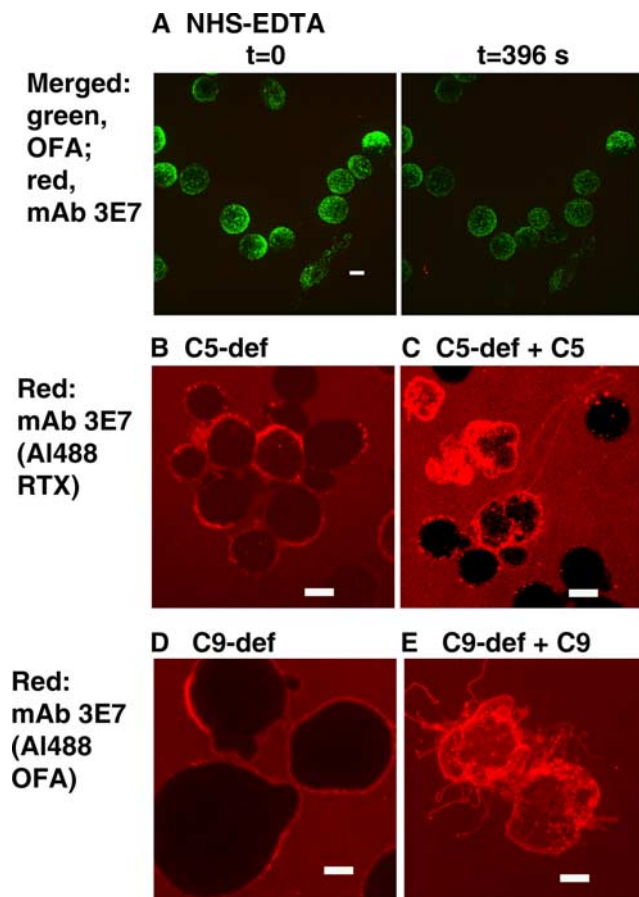
OFA is more effective than RTX in promoting blebbing, streaming, and cell killing

We directly compared OFA and RTX with respect to the kinetics at which they induce blebbing and streamer formation. Daudi cells were opsonized with either Al488 RTX or with Al488 OFA, washed, chilled on ice, and then combined with NHS containing Al647 mAb 3E7 and analyzed by SDCM. Images from the movie (supplemental movie 5) obtained using the OFA-opsonized cells are shown in Fig. 4*A* at three time points. Streamers are first seen in this movie after ~114 s. In the corresponding movie for RTX-opsonized cells (supplemental movie 6), streamers are not discernible until after ~418 s have elapsed (Fig. 4*B*). The images also reveal that at zero time (~2 min after mixing cells with NHS) more C3b is deposited on the OFA-opsonized cells than on the RTX-opsonized cells, as evidenced by the greater intensity of yellow color on the OFA-opsonized cells, due to greater binding of Al647 mAb 3E7. In both movies, the cells were treated in an identical manner to insure a valid comparison; the samples were

Table I. *Summary of effects of various reagents on generation of streamers*

Experimental Conditions			Streaming Results[a]
C Source	Addition	Function	
50% NHS		Positive control	5
50% C5-depleted serum		MAC formation is blocked	0
50% C5-depleted serum	C5	MAC formation is restored	3
50% C9-depleted serum		MAC formation is blocked	0
50% C9-depleted serum	C9	MAC formation is restored	3
50% NHS	Cytochalasin D	Inhibits actin polymerization	1
25% NHS	Nocodazole	Inhibits microtubule formation	4
None	Azide	Generates microvilli	0
None	Melittin	Alternative pore former	2
50% citrated plasma		Clotting proteins intact; C can be activated	4
50% NHS	Protein kinase C and MEK inhibitors (see text)	Inhibit release of C9-containing vesicles	5

[a] See *Materials and Methods* for scoring system.

prechilled on ice and then placed on the slide to begin the movies. We confirmed that there was indeed more rapid deposition of C3b on OFA-opsonized B cells in >10 similar experiments as well as in flow cytometry experiments (not shown).

We also performed experiments comparing the kinetics of C-mediated killing of Daudi cells opsonized with either Al488 RTX or with Al488 OFA. The opsonized cells were combined with NHS containing Al647 mAb 3E7 and the viability dye 7-AAD, whose fluorescence does not overlap with that of the Al488- and Al647-labeled mAbs. Three-color images as well as the complete SDCM movie for OFA-opsonized cells indicate that killing occurs rapidly (Fig. 5*A* and supplement 7); the 7-AAD stain, which appears blue (pseudocolor) in the merged images or as white in the single-color images, is first clearly visible within the cells at $t = 0$ s for the OFA-opsonized cells, and staining by 7-AAD is preceded by the appearance of the streamers. In contrast to the results with OFA, uptake of 7-AAD is not seen until 293 s for RTX-opsonized cells (supplement 8 and Fig. 5*B*). These differences in the kinetics of killing and streaming between OFA and RTX were highly reproducible, and faster killing was also verified by flow cytometry studies (not shown). However, after an incubation of 15 min at 37°C, Daudi cell killing mediated by RTX and OFA in the presence of NHS was quite comparable: 93 and 97%, respectively. In studies with ARH77 cells, opsonization with OFA also led to much faster deposition of C3b on the cells compared with C3b deposition mediated by RTX (not shown), and OFA also mediated substantial cell killing (39). In contrast, RTX was not able to promote complement-mediated

killing of ARH77 cells even after incubation for several hours in the presence of NHS.

Analyses with primary B cells

We extended our studies to primary B cells. B cells from a normal individual were reacted with OFA and NHS and then examined by SDCM; both streaming and blebbing were demonstrable on approximately half of the cells (Fig. 6, *A* and *B*). SDCM analyses of OFA-opsonized B cells from a representative CLL patient revealed extensive C3b deposition, and ~3% of the cells showed streaming and blebbing (Fig. 6, *C* and *D*). No streaming and only very weak C3b deposition was detected for cells reacted with RTX (not shown). Because of this low frequency of streaming we tested subsequent samples from seven additional CLL patients using FM, which allows for rapid screening of large numbers of cells. CLL cells from one patient expressed little, if any, CD20 and had absolutely no streaming or blebbing (not shown). However, streaming and blebbing were clearly demonstrable in both bright field and fluorescence for the other CD20^{+} CLL cells treated with OFA and NHS, although the levels were quite variable (Fig. 7, *A–F*, and Table II). We also evaluated CD20 levels and mAb-mediated CDC for selected CLL samples. Although streaming was more modest than seen for Daudi cells, OFA was far more effective at generating streamers than RTX. In agreement with the report of Teeling et al. (31), but for one exception where the % killing was comparable, OFA promoted greater CDC than RTX, although we only examined a limited number of samples.

FIGURE 4. Opsonization of cells with OFA promotes more rapid blebbing and streamer formation than opsonization with RTX. *A*, Daudi cells were opsonized with Al488 OFA and then chilled on ice before reaction with NHS and Al647 mAb 3E7. The chilled mixture was then placed on the heated (37°C) microscope stage and analyzed by SDCM; merged 488 nm/647 nm images. Also, see supplemental movie 5. *B*, Same procedure as in *A*, but Al488 RTX was used instead of Al488 OFA. Also, see supplemental movie 6.
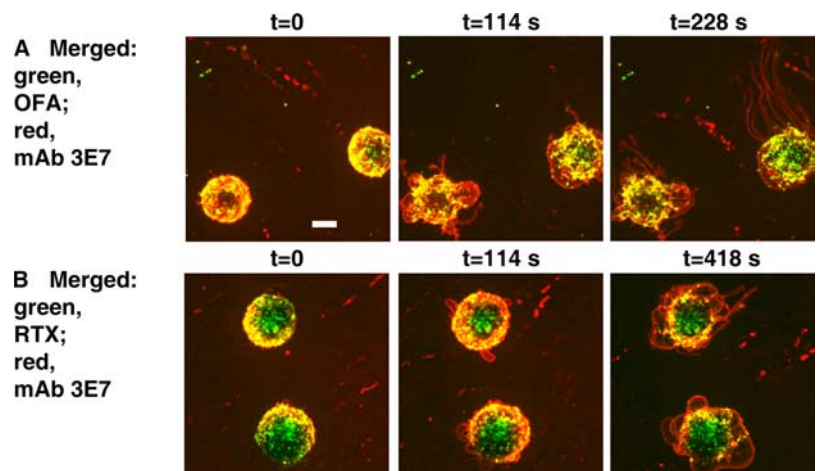
FIGURE 5. Opsonization of cells with OFA mediates more rapid C-mediated cytotoxicity than opsonization with RTX. *A*, Daudi cells were opsonized with Al488 OFA, then reacted with NHS, Al647 mAb 3E7, and 7-AAD (which stains dead cells). The three-color merged images (488 nm/568 nm/647 nm) are shown. OFA is green, mAb 3E7 is red and 7AAD is false blue. To aid in identifying dead cells, the 568 nm images alone are also shown (black and white, with white representing 7-AAD staining). Also, see supplemental movie 7. *B*, Same procedure as in *A*, but Al488 RTX was used instead of Al488 OFA. Also, see supplemental movie 8.
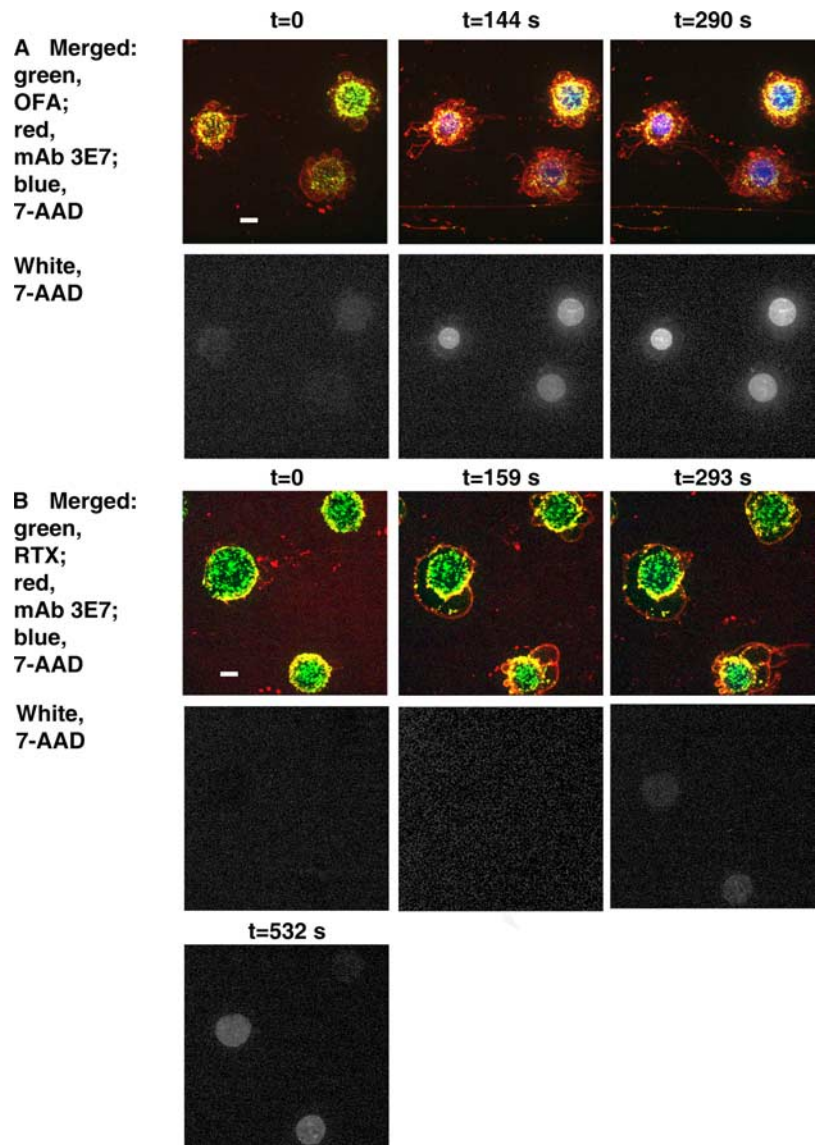
Characterization of the streamers

As we have noted, Fig. 1 shows that C3b is present on the streamers. We performed several additional experiments that focused on identifying other constituents in the streamers. We prepared RTX-opsonized Daudi cells and reacted them with NHS and Al647 mAb 3E7 in the presence of Al488 phalloidin, which binds to polymerized actin. As the streamers develop, they clearly are stained by the phalloidin (Fig. 8*A*), indicating they contain polymerized actin; it is also interesting to note that there is much weaker binding of phalloidin to the cells which lacked streamers. Moreover, pretreatment of Daudi cells with cytochalasin D, which inhibits actin polymerization, suppresses OFA-mediated streamer formation considerably, although some of the cells do release vesicles (Fig. 8*B*, Table I, and supplemental movie 9). In addition, although cytochalasin D inhibits streaming by nucleated cells, nocodazole does not (Table I), indicating that the streaming reaction does not appear to require the formation of microtubules.

To determine whether streamers contain plasma membrane lipids, Daudi cells were first labeled with the membrane dye PKH 26 and then opsonized with Al647 RTX and reacted with NHS. The PKH 26 signal (488 nm image; Fig. 8*C*) and the red Al647 RTX signals are clearly evident in the streamers. In summary, the streamers appear to include bound CD20 mAbs, deposited C3b/iC3b, membrane lipids and polymerized actin. We evaluated C activation both in bright field (phase imaging, white light) as well as by fluorescence. OFA-opsonized Daudi cells were incubated with NHS in the presence of Al488 mAb 3E7; the resulting SDCM movies (supplemental movies 10 and 11) as well as the images (Fig. 9, *A* and *B*) clearly demonstrate a concordance between the 488 nm and bright field images. The fact that the streamers can be visualized in bright field is consistent with the idea that the streamers likely contain substantial amounts of cell membrane and associated proteins.

We observed a general correlation between streaming and uptake of the viability dye 7-AAD, i.e., cells with visible streamers usually take up the viability dye and cells which take up the viability dye usually exhibit streaming. However, based on both SDCM and FM experiments, we also observed Daudi and CLL cells that were killed and never exhibited streaming. The differential between streaming and killing can be increased by treating Daudi cells with cytochalasin D. Streaming is largely suppressed by such treatment (Table I, Fig. 9*B*, and supplemental movie 9) but there is no effect on killing. For example, killing of Daudi cells mediated by Al488 RTX in NHS was 73 ± 1% for untreated cells, and 76 ± 1% for cells first reacted with cytochalasin D.

A B cells from normal
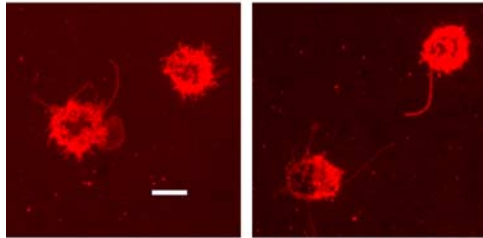
B B cells from CLL Patient 1
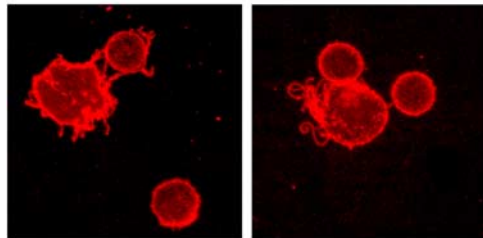
Red: mAb 3E7

FIGURE 6. Reaction of normal human B cells and CLL cells with OFA generates streamers. *A, top two panels,* Purified B cells from a normal individual were opsonized with OFA and then reacted with 50% NHS and Al647 mAb 3E7. The 647 nm images are representative of ~50% of the cells that were examined. The other cells were stained red, but did not show blebs or streamers. *B, bottom two panels,* Purified CLL cells from patient number 1 were opsonized with OFA and then reacted with 50% NHS and Al647 mAb 3E7.

Table II. *CLL patient samples: summary of CD20 levels, percent streaming, and percent CDC*

Patient ID	% CD20[a]	Estimated % Streaming	% CDC[b] ± SD	
			OFA	RTX
1	25	3	ND	ND
2	5	3–5	65 ± 2	11 ± 1
3	8	3–5	ND	ND
4	40	30	ND	ND
5	54	30	89 ± 1	78 ± 1
6	5	5	70 ± 1	1 ± 1
7	7	5	48 ± 7	2 ± 1

[a] Mean FL1 values for cells opsonized with Al488 RTX were converted to molecules of equivalent soluble fluorochrome and compared to Daudi cells treated identically.
[b] With 50% NHS, 37° C, 30 min.

Extension of these findings to other CD20 mAb and to additional targets

Several CD20 mAbs that do not activate C have been described, and we tested the ability of two such mAbs, 11B8 (31) and B1 (35), to induce streamer formation. mAb 11B8 and B1 are Type II CD20 mAbs that are able to directly kill cells in the absence of C by mediating either apoptosis or autophagy (27, 31, 40). We tested the potential of these mAbs, and of F(ab′)$_2$ of RTX (which do not
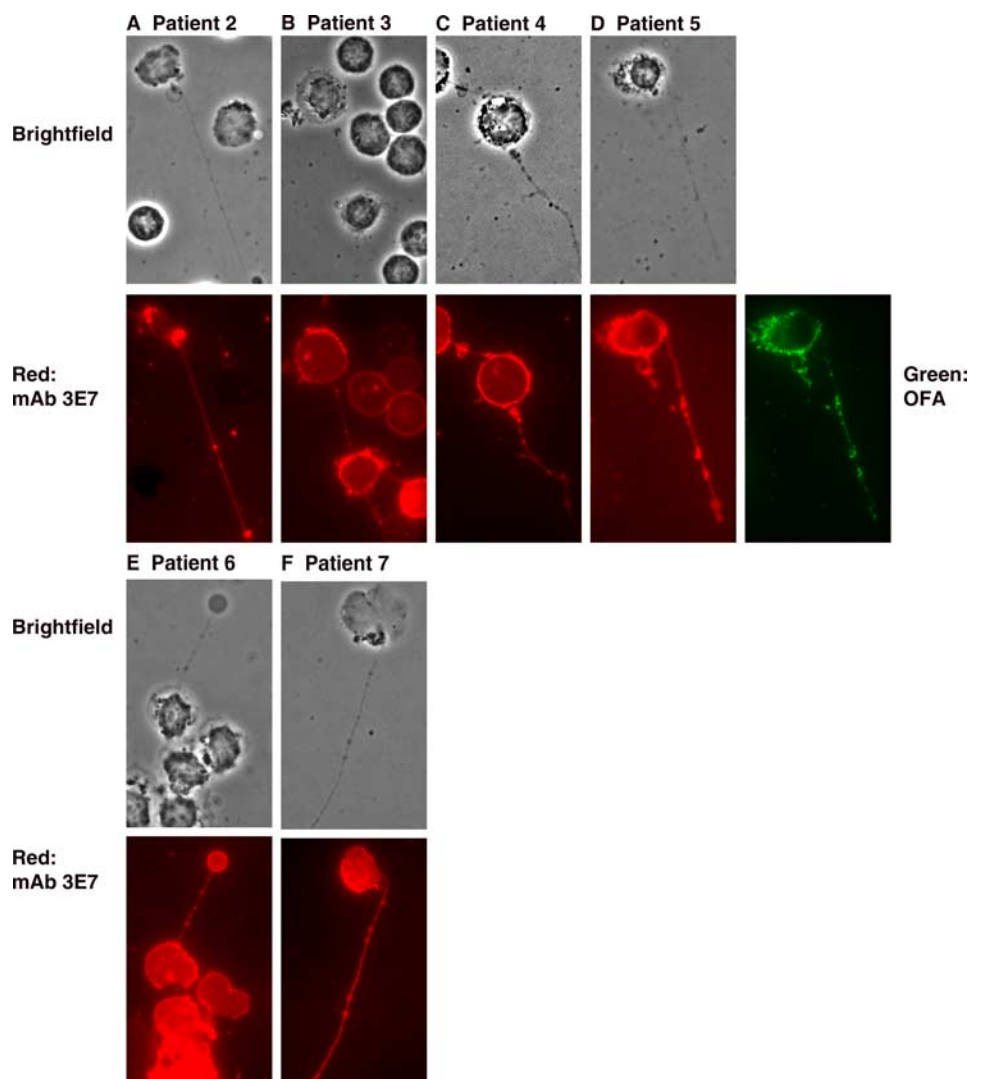
FIGURE 7. FM reveals streaming and blebbing by CLL cells reacted with OFA in NHS. *A–C,* For patients 2–4, respectively, cells were opsonized with OFA and then reacted with NHS and Al594 mAb 3E7 and examined at once or briefly incubated at 37°C for periods of 2–5 min. Representative images are provided. *D–F,* Cells from patients 5–7 were reacted with Al488 OFA (patient 5) or with OFA (patients 6–7) and with Al594 mAb 3E7 in 50% NHS, and then evaluated for green (Al488) or red (Al594) fluorescence.

FIGURE 8. Streamers contain both polymerized actin and membrane lipids, and cytochalasin D inhibits streamer formation and promotes release of vesicles. *A,* Daudi cells were opsonized with RTX and then reacted with NHS and Al488 phalloidin and Al647 mAb 3E7; 488 nm image shows phalloidin at the indicated times. *B,* Daudi cells were preincubated with 2.5 μM cytochalasin D, opsonized with unlabeled OFA, and then reacted with NHS and Al647 mAb 3E7. The 647 nm image shows mAb 3E7 at the indicated times. See supplemental movie 9. *C,* Daudi cells were stained with PKH 26, opsonized with Al647 RTX, and then reacted with NHS. The 488 nm (green) image shows PKH 26, and the 647 nm (red) image shows RTX.
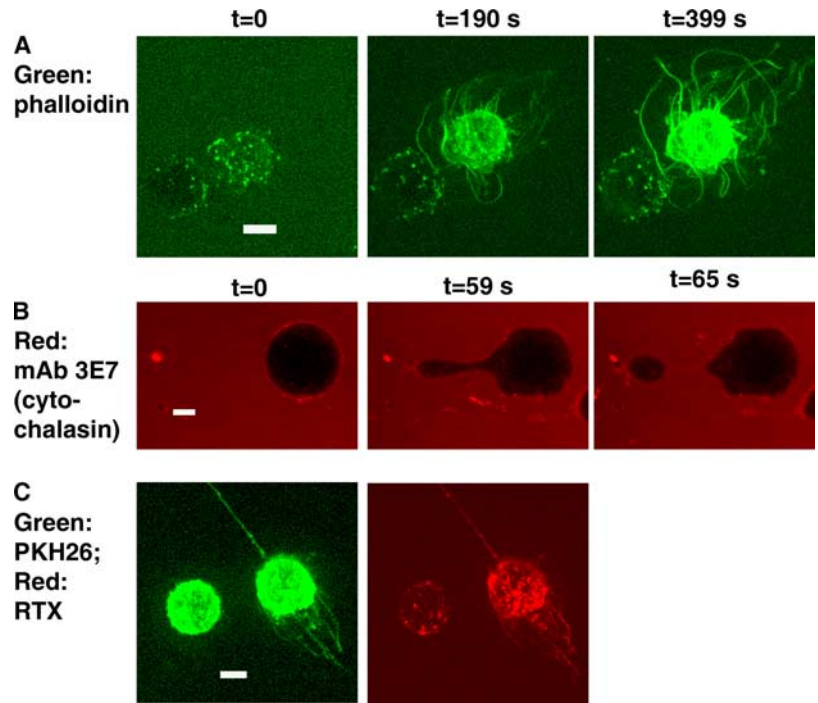
activate C), to induce streamers in a further test of the importance of C activation in this reaction. Opsonization of Daudi cells with these reagents, followed by incubation in NHS containing mAb 3E7, led to no streamer formation whatsoever (not shown). These results, along with our findings with NHS-EDTA, C5-deficient and C5-reconstituted sera, and C9-deficient and C9-reconstituted sera, argue that C activation is critical for streamer formation and is quite likely mediated by the same agent that lyses cells, the MAC.

We next investigated whether streamer production can occur in non-nucleated cells, specifically in sheep erythrocytes (E), the usual substrate for assays of C activation (41). We first opsonized the E with rabbit hemolysin (28), then stained the plasma membrane of the opsonized cells (EA) with PKH 26 (37), and then examined these cells, in the presence of varying amounts of NHS, by both SDCM analysis and FM. Streamer formation is clearly evident (Fig. 10*A*), and streaming is completely abrogated in the presence of NHS-EDTA or heat-inactivated NHS (not shown), thus verifying the requirement for C activation. However, the

streamers did not take up the Al488 phalloidin stain (not shown), and cytochalasin D did not block formation of streamers, suggesting the absence of polymerized actin in the streamers formed on EA. Also, in contrast to our findings with Daudi and ARH77 cells, we did not detect any blebbing in the Ab opsonized sheep E. These results suggest that there are differences between the streamers in non-nucleated cells and those observed with nucleated cells.

Investigation of possible mechanisms of streamer formation

Our results strongly suggest that the MAC is the key mediator of streamer production. We investigated this hypothesis using another membrane pore-forming agent, bee venom melittin (42, 43). We reacted Daudi cells, which were opsonized with Al647 OFA for readout, with melittin in the absence of NHS to determine whether melittin can induce streaming independent of C. Melittin-treated Daudi cells indeed exhibit streaming in medium alone (Fig. 10*B*), although not as many cells have streamers compared with cells opsonized with OFA and reacted with NHS. These findings add further
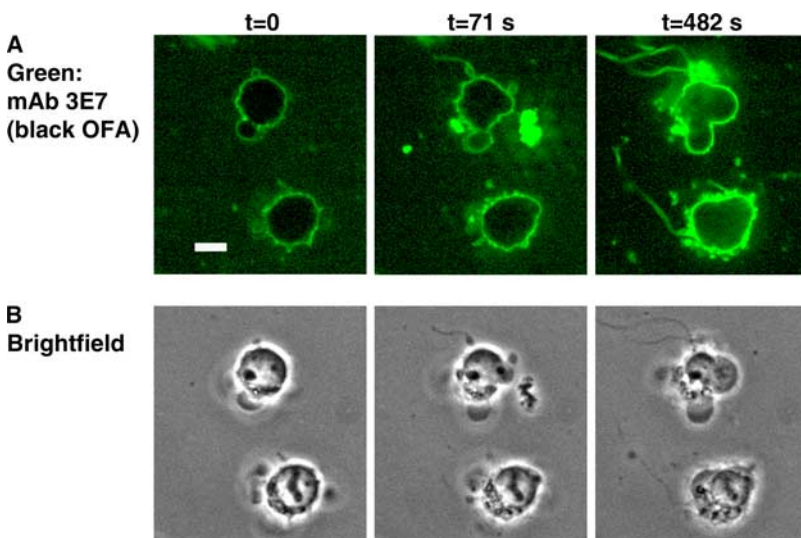

FIGURE 9. Streamers can be observed in bright field (phase imaging), and have the same appearance as streamers detected by fluorescence. Daudi cells were opsonized with OFA, and then reacted with NHS and Al488 mAb 3E7. *A,* 488 nm image. *B,* bright field images of the same field as in *A.* See supplemental movies 10 and 11.

A   Red, mAb 3E7
(Sheep E/hemolysin/NHS)

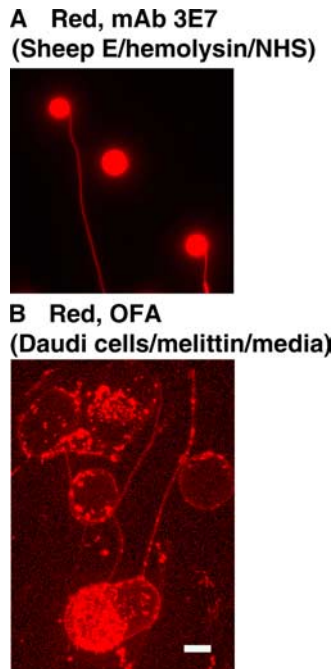
B   Red, OFA
(Daudi cells/melittin/media)

FIGURE 10. Two examples of the streaming reaction in other systems. *A.* Sheep E, dyed with PKH 26, were opsonized with hemolysin and then briefly reacted with NHS (final concentration of 8%) at 37°C. The cells were examined by FM (×100 magnification). *B,* Daudi cells were opsonized with Al647 OFA, and then reacted with 7.5 μM mellitin in RPMI 1640 media (no C present) and examined by SDCM; 647 nm image shows OFA.

support to the hypothesis that pore-formation by the MAC is responsible for streamer production which occurs upon C activation.

Azide has been reported to induce formation of microvilli in nucleated cells (44). To determine whether streaming is related to microvilli formation, we reacted Daudi cells with azide in the absence of NHS. Azide was unable to induce streaming (Table I), suggesting that streaming and microvilli formation are fundamentally different processes.

Reaction of nucleated cells with sublytic amounts of C can lead to the rapid release of vesicles that are enriched in the MAC, and this process appears to be mediated by the mitochondrial heat-shock protein 70, also called mortalin (45–48). It is important to determine whether the streamer production we have seen could be related to, or is simply another manifestation of, the vesicle release process described by Morgan, Fishelson, and their colleagues (45–47). Mortalin-mediated release of C9-containing vesicles can be blocked by several inhibitors of protein kinase C and extracellular signal-related protein kinase (MEK) (46, 47). We tested the ability of several such inhibitors of vesicle release to block streaming: OFA-opsonized Daudi cells, pretreated with the inhibitors bisin-dolylmaleimide I, sphingosine, calphostin C, polymyxin B sulfate, Go6976, or PD98059, showed no reduction in streaming when incubated in the presence of NHS (Table I). Thus, our results indicate that streaming is quite likely to be an entirely separate phenomenon from vesicle release.

Discussion

The molecular steps in the C cascades have been defined in great detail, and the mechanism by which the MAC of C promotes killing of non-nucleated cells has been delineated (41). However, the processes that can occur when C attack is directed to nucleated cells, i.e., cells which can more effectively defend against both C3b deposition and penetration of the membrane by multiple hits by the

MAC, are likely to be far more complex and may vary between cell types (see Refs. 11, 49–53 and references therein). For example, a considerable body of evidence indicates that one of the ways that cancer cells inhibit C-mediated killing is by expressing increased levels of C control proteins (11, 49–53). Moreover, when sublytic amounts of C are used to attack nucleated cells, the cells can respond by implementing strategies to enhance their resistance to subsequent assaults by C (46, 48, 53).

We initiated the present studies to investigate the real-time dynamics of discreet steps in C activation, in particular C3b deposition on mAb-opsonized cells. Careful inspection of the SDCM movies confirms that most of the C3b that initially deposits on the cells is indeed located in close proximity to bound RTX, thus, generating yellow-orange patterns due to colocalization of red mAb 3E7 with green cell-bound RTX (Figs. 1, *A–C,* 4*B,* and 5*B*). The patterns associated with cells opsonized with OFA are similar but not identical (Fig. 2*A,* 4*A,* and 5*A*); this mAb promotes more rapid C3b deposition and C-mediated killing of the cells than RTX, and our flow cytometry experiments (not shown) indicate that as the cells are penetrated by the MAC and killed, OFA dissociates from the cells.

In the presence of C, OFA induces streaming on ARH77 cells much more effectively than RTX, and it is likely this effect is due to the superior ability of this mAb to activate C when it binds to CD20 on targeted cells. RTX is not able to promote C-mediated killing of ARH77 cells, presumably because these cells express high levels of the C control proteins CD55 and CD59. Indeed, Teeling et al. (31, 32) has reported that OFA overcomes the resistance of these cells to C-mediated killing, and we have confirmed their observations (39). Teeling et al. (32) has also presented evidence indicating that the small loop epitope on CD20 that is bound by OFA is located much closer to the B cell membrane than the large loop epitope bound by RTX. Binding of multiple copies of OFA to these epitopes on B cells, followed by initiation of C activation, should, therefore, allow for shorter diffusion times for nascent activated C3b to reach the cell surface, thus, allowing for more efficient C3b deposition and subsequent amplification of C activation (41, 49, 53). This mechanism likely explains the increased C3b deposition and more rapid streaming and blebbing we observed for OFA compared with RTX.

The major findings in this paper center on the observation of two phenomena: blebbing and the production of streamers by the cells. Both of these processes require binding to the cell of a C-fixing CD20 mAb, RTX or OFA, followed by contact of these cells with an intact C cascade. Although blebbing can be induced in cells by a variety of mechanisms, our review of the literature did not reveal any citations in which rapid membrane blebbing (~5 min or less) induced by C was reported in real time with nucleated cells. Several investigators have reported C-induced morphological changes on a variety of different target cells, based on electron microscopy analyses of fixed tissue or cells (54–56). However, the kinetics of formation as well as the physical properties of the reported blebs in these cited studies are quite different from the blebbing and streaming phenomena we describe in this report; the changes described in these previous studies appear to be most consistent with the release of membrane vesicles containing C9.

The formation of streamers, which occurs as a consequence of C activation, has not been previously reported. The streamers can be quite long and are substantial enough to be seen in bright field; in many cases, they correspond in length to more than two cell diameters (Figs. 2–4 and 7–10), indicating that they are not simply microvilli. Indeed, reaction of the cells with azide, previously reported

to induce microvilli formation (44), does not produce streamers (Table I). Streamer formation also does not appear to be related to mortalin-mediated release of C9-containing vesicles, because inhibitors of vesicle release do not block formation of streamers (Table I). The streamers also appear to be quite fragile, and, in fact, we never observed streamers when the opsonized cells were reacted with C and then washed (which employs harsh treatment, such as vortexing and centrifugation) before they were examined by FM or by SDCM (10, 19, 28). This may explain why streamers have not previously been reported on cells following C attack.

Several lines of evidence suggest that after binding of RTX or OFA to the cell, C activation followed by penetration of the cell membrane by the pore-forming agent of C, the MAC, promotes blebbing as well as formation of the streamers. For example, these reactions do not occur in media alone, or in heat-inactivated NHS or in NHS-EDTA (Fig. 3A). Although C3b deposition occurs in C5- and in C9-deficient serum (Fig. 3, B and D), streamers are not produced unless the missing C components are added back to the respective sera (Fig. 3 and Table I). Binding of non-C-fixing CD20 mAbs to cells does not produce streamers, and OFA, which activates C more effectively than does RTX (31–33), induces more C3b deposition, blebbing, streaming, and killing of opsonized cells than is induced by RTX (Figs. 4 and 5 and Table II). Moreover, OFA mediates these reactions more rapidly than does RTX. Additional evidence in support of the hypothesis that penetration of the cell membrane by the MAC initiates streamer formation stems from the observation that use of mellittin, in the absence of C, can also induce streaming (Fig. 10B). Finally, although it has been suggested that binding of RTX to B cells induces apoptosis (57–59), the evidence supporting this hypothesis has been questioned (27). The dynamic and rapid changes we have described for RTX-opsonized cells demonstrate an absolute requirement for C, and, therefore, we can exclude any role for apoptosis in the observed blebbing, streaming, and killing reactions.

We were able to demonstrate streaming and blebbing on both normal B cells and on CLL B cells opsonized with OFA, but, in many cases, these structures were detected in only a small fraction of the CLL cells (Figs. 6 and 7). CD20 levels were lower on the patient cells than on Daudi cells (Table II), which may provide one explanation for the decreased number of streamer-positive cells. However, we did see a general correlation between killing and streaming (Table II). Indeed, OFA was more effective than RTX at mediating CDC, and this was also manifest in increased levels of streaming. It is also likely that expression of C control proteins CD55 and CD59 on the cells as well as plasma levels of Factors H and I will modulate the potential of OFA to promote robust C activation (11, 31, 49, 60) and, thus, induce streaming and blebbing on the cells.

B cells do not express the C5a receptor (61), and, thus, streamers are not likely to be a cellular response to C5a production. Moreover, we also observe streaming in plasma obtained from blood anti-coagulated with citrate (Table I), thus, indicating that streamers are not related to any clotting proteins. However, formation of actin polymers is likely part of the mechanisms of streaming, because streamer formation can be substantially blocked by preincubating cells with cytochalasin D (Fig. 8B), and, in addition, the streamers can be stained with phalloidin (Fig. 8A), which binds to polymerized actin. It is possible that streamer formation is related to formation of filopodia, actin filaments that extend from cells and are first observed 5 min or later after stimulation with Cdc42, a member of the Rho family of GTPases (62–64). However, streamers in our studies appear to be longer than filopodia, and in many of the experiments that made use of OFA, we detected large numbers of streamers and blebs in a very brief period of time, in 1–2

min or less. Whether the attack on a cell by the MAC provides an early signal that stimulates the Cdc42 pathway will be addressed in future experiments using cells in which Cdc42 protein activity is blocked (64).

The results for non-nucleated cells, EA, exposed to C are similar, but not identical, with the results obtained with nucleated cells. C activation on EA also produces streamers (Fig. 10A), but, as we have noted, we did not observe blebbing. Moreover, some of the properties of these streamers appear to be different from those seen with nucleated cells, including the apparent lack of staining of the streamers by Al488 phalloidin, and the inability of cytochalasin D to block streamer formation on EA reacted with NHS.

The broader implications of our findings with respect to the use of mAbs in cancer immunotherapy remain to be delineated. However, we have observed streaming in the presence of C in several other mAb-target cancer cell systems (results not shown, to be reported separately) in addition to the RTX/OFA anti-CD20 system reported here, suggesting that streaming may be a general phenomenon associated with C attack.

In summary, we have used SDCM to examine the real-time dynamics of C activation promoted by the binding of either RTX or OFA to CD20-positive cells. Activation of C by these cells induces rapid changes in cell shape and morphology, and leads to formation of streamers, which contain polymerized actin, membrane lipids, bound mAbs, and deposited C3b fragments. The terminal phase of the C pathway generates the MAC, a pore-forming agent that can penetrate cell membranes, and our results suggest that the MAC is the primary mediator of these changes. These real-time analyses reveal several new phenomena that occur as a consequence of the attack of C on mAb-opsonized nucleated cells. The molecular mechanisms that induce these effects are under investigation.

Disclosures
The authors have no financial conflict of interest.

References
1. Maloney, D. G., A. J. Grillo-López, C. A. White, D. Bodkin, R. J. Schilder, J. A. Neidhart, N. Janakiraman, K. A. Foon, et al. 1997. IDEC-C2B8 (Rituximab) anti-CD20 monoclonal antibody therapy in patients with relapsed low-grade non-Hodgkin's lymphoma. *Blood* 90: 2188–2195.
2. McLaughlin, P., A. J. Grillo-Lopez, B. K. Link, R. Levy, M. S. Czuczman, M. E. Williams, M. R. Heyman, I. Bence-Bruckler, C. A. White, F. Cabanillas, et al. 1998. Rituximab chimeric anti-CD20 monoclonal antibody therapy for relapsed indolent lymphoma: half of patients respond to a four-dose treatment program. *J. Clin. Oncol.* 16: 2825–2833.
3. Maloney, D. G. 1999. Preclinical and phase I and II trials of Rituximab. *Semin. Oncol.* 26: 74–78.
4. McLaughlin, P. 2001. Rituximab: perspective on single agent experience, and future directions in combination trials. *Crit. Rev. Oncol. Hematol.* 40: 3–16.
5. Johnson, P., and M. Glennie. 2003. The mechanisms of action of rituximab in the elimination of tumor cells. *Semin. Oncol.* 30: 3–8.
6. Silverman, G. J., and S. Weisman. 2003. Rituximab therapy and autoimmune disorders: prospects for anti-B Cell therapy. *Arthritis Rheum.* 48: 1484–1492.
7. Edwards, J. C. W., and G. Cambridge. 2006. B-cell targeting in rheumatoid arthritis and other autoimmune diseases. *Nat. Rev. Immunol.* 6: 394–403.
8. Cohen, S. B., P. Emery, M. W. Greenwald, M. Dougados, R. A. Furie, M. C. Genovese, E. C. Keystone, J. E. Loveless, G. R. Burmester, M. W. Cravets, et al. 2006. Rituximab for rheumatoid arthritis refractory to anti-tumor necrosis factor therapy: results of a multicenter, randomized, double-blind, placebo-controlled, phase III trial evaluating primary efficacy and safty at twenty-four weeks. *Arthritis Rheum.* 54: 2793–2806.
9. Reff, M. E., K. Carner, K. S. Chambers, P. C. Chinn, J. E. Leonard, R. Raab, R. A. Newman, N. Hanna, and D. R. Anderson. 1994. Depletion of B cells in vivo by a chimeric mouse human monoclonal antibody to CD20. *Blood* 83: 435–445.
10. Harjunpää, A., S. Junnikkala, and S. Meri. 2000. Rituximab (anti-CD20) therapy of B-cell lymphomas: direct complement killing is superior to cellular effector mechanisms. *Scand. J. Immunol.* 51: 634–641.
11. Golay, J., L. Zaffaroni, T. Vaccari, M. Lazari, G. Borleri, S. Bernasconi, F. Tedesco, A. Rambaldi, and M. Introna. 2000. Biologic response of B lymphoma cells to anti-CD20 monoclonal antibody rituximab in vitro: CD55 and CD59 regulate complement mediated cell lysis. *Blood* 95: 3900–3908.

12. Clynes, R. A., T. L. Towers, L. G. Presta, and J. V. Ravetch. 2000. Inhibitory Fc receptors modulate in vivo cytotoxicity against tumor targets. *Nat. Med.* 6: 443–446.

13. Cartron, G., L. Dacheux, G. Salles, P. Solal-Celigny, P. Bardos, P. Colombat, and H. Watier. 2002. Therapeutic activity of humanized anti-CD20 monoclonal antibody and polymorphism in IgG Fc receptor FcγRIIIa gene. *Blood* 99: 754–758.

14. Manches, O., G. Lui, L. Chaperot, R. Gressin, J. P. Molens, M. C. Jacob, J. J. Sotto, D. Leroux, J. C. Bensa, and J. Plumas. 2002. In vitro mechanisms of action of rituximab on primary non-Hodgkin's lymphomas. *Blood* 101: 949–954.

15. Cragg, M. S., S. M. Morgan, H. T. C. Chan, B. P. Morgan, A. V. Filatov, P. W. M. Johnson, R. R. French, and M. J. Glennie. 2003. Complement-mediated lysis by anti-CD20 mAb correlates with segregation into lipid "rafts." *Blood* 101: 1045–1052.

16. Di Gaetano, N., E. Cittera, R. Nota, A. Vecchi, V. Grieco, E. Scanziani, M. Botto, M. Introna, and J. Golay. 2003. Complement activation determines the therapeutic activity of Rituximab in vivo. *J. Immunol.* 171: 1581–1587.

17. Weng, W. K., and R. Levy. 2003. Two immunoglobulin G fragment C receptor polymorphisms independently predict response to Rituximab in patients with follicular lymphoma. *J. Clin. Oncol.* 21: 3940–3947.

18. Golay, J., M. Manganini, V. Facchinetti, R. Gramigna, R. Broady, G. Borleri, A. Rambaldi, and M. Introna. 2003. Rituximab-mediated antibody-dependent cellular cytotoxicity against neoplastic B cells is stimulated strongly by interleukin-2. *Haematologica* 88: 1002–1012.

19. Kennedy, A. D., M. D. Solga, T. A. Schuman, A. W. Chi, M. A. Lindorfer, W. M. Sutherland, P. L. Foley, and R. P. Taylor. 2003. An anti-C3b(i) mAb enhances complement activation, C3b(i) deposition, and killing of CD20$^+$ cells by Rituximab. *Blood* 101: 1071–1079.

20. Gaetno, N. D., E. Cittera, R. Nota, A. Vecchi, V. Grieco, E. Scanziani, M. Botto, M. Introna, and J. Golay. 2003. Complement activation determines the therapeutic activity of rituximab in vivo. *J. Immunol.* 171: 1581–1587.

21. Dall'Ozzo, S., S. Tartas, G. Paintaud, G. Cartron, P. Colombat, P. Bardos, H. Watier, and G. Thibault. 2004. Rituximab-dependent cytotoxicity by natural killer cells: influence of FCGR3A polymorphism on the concentration-effect relationship. *Cancer Res.* 64: 4664–4669.

22. Uchida, J., Y. Hamaguchi, J. A. Oliver, J. V. Ravetch, J. C. Poe, K. M. Haas, and T. F. Tedder. 2004. The innate mononuclear phagocyte network depletes B lymphocytes through Fc receptor-dependent mechanisms during anti-CD20 antibody immunotherapy. *J. Exp. Med.* 199: 1659–1669.

23. Bowles, J. A., and G. J. Weiner. 2005. CD16 polymorphisms and NK activation induced by monoclonal antibody-coated target cells. *J. Immunol. Methods* 304: 88–99.

24. Lefebvre, M. L., S. W. Krause, M. Salcedo, and A. Nardin. 2006. Ex vivo-activated human macrophages kill chronic lymphocytic leukemia cells in the presence of Rituximab: mechanism of antibody-dependent cellular cytotoxicity and impact of human serum. *J. Immunother.* 29: 388–397.

25. Hamaguchi, Y., Y. Xiu, K. Komura, F. Nimmerjahn, and T. F. Tedder. 2006. Antibody isotype-specific engagement of Fcγ receptors regulates B lymphocyte depletion during CD20 immunotherapy. *J. Exp. Med.* 203: 743–753.

26. Tedder, T. F., A. Baras, and Y. Xiu. 2006. Fcγ receptor-dependent effector mechanisms regulate CD19 and CD20 antibody immunotherapies for B lymphocyte malignancies and autoimmunity. *Semin. Immunol.* 28: 351–364.

27. Glennie, M. J., R. French, M. S. Cragg, and R. P. Taylor. 2007. Mechanisms of killing by anti-CD20 monoclonal antibodies. *Mol. Immunol.* 44: 3823–3837.

28. Kennedy, A. D., P. V. Beum, M. D. Solga, D. J. DiLillo, M. A. Lindorfer, C. E. Hess, J. J. Densmore, M. E. Williams, and R. P. Taylor. 2004. Rituximab infusion promotes rapid complement depletion and acute CD20 loss in chronic lymphocytic leukemia. *J. Immunol.* 172: 3280–3288.

29. Beum, P. V., M. A. Lindorfer, B. E. Hall, T. C. George, K. Frost, P. J. Morrissey, and R. P. Taylor. 2006. Quantitative analysis of protein co-localization on B cells opsonized with rituximab and complement using the ImageStream multispectral imaging flow cytometer. *J. Immunol. Methods* 317: 90–99.

30. Emanuele, M. J., and P. T. Stukenberg. 2007. Xenopus Cep57 is a novel kinetochore component involved in microtubule attachment. *Cell* 130: 893–905.

31. Teeling, J., R. R. French, M. S. Cragg, J. van den Brakel, M. Pluyter, H. Huang, C. Chan, P. W. Parren, C. E. Hack, M. Dechant, et al. 2004. Characterisation of new human CD20 monoclonal antibodies with potent cytolytic activity against non-Hodgkin's lymphomas. *Blood* 104: 1793–1800.

32. Teeling, J. L., W. J. M. Mackus, L. J. J. M. Wiegman, J. H. N. van den Brakel, S. A. Bees, R. R. French, T. van Meerten, S. Ebeling, T. Vink, J. W. Slootstra, et al. 2006. The biological activity of human CD20 monoclonal antibodies is linked to unique epitopes on CD20. *J. Immunol.* 177: 362–371.

33. Coiffier, B., H. Tilly, L. M. Pedersen, T. Plesner, H. Frederiksen, M. H. J. Van Oers, J. Wooldridge, J. Kloczko, J. Holowiecki, A. Hellmann, et al. 2005. HuMax CD20 fully human monoclonal antibody in chronic lymphocytic leukemia: early results from an ongoing Phase I/II clinical trial. *Blood* 106: 135a.

34. Beum, P. V., A. D. Kennedy, M. E. Williams, M. A. Lindorfer, and R. P. Taylor. 2006. The shaving reaction: Rituximab/CD20 complexes are removed from mantle cell lymphoma and chronic lymphocytic leukemia cells by THP-1 monocytes. *J. Immunol.* 176: 2600–2609.

35. Cardarelli, P. M., M. Quinn, D. Buckman, Y. Fang, D. Colcher, D. King, C. Bebbington, and G. Yarranton. 2002. Binding to CD20 by anti-B1 antibody or F(ab′)2 is sufficient for induction of apoptosis in B-cell lines. *Cancer Immunol. Immunother.* 51: 15–24.

36. Whaley, K., and J. North. 1997. Haemolytic assays for whole complement activity and individual components. In *Complement: A Practical Approach.* A. W. Dodds and R. B. Sim, eds. IRL at Oxford University Press, Oxford, pp. 19–48.

37. Henderson, A. L., M. A. Lindorfer, A. D. Kennedy, P. L. Foley, and R. P. Taylor. 2002. Concerted clearance of immune complexes bound to the human erythrocyte complement receptor: development of a heterologous mouse model. *J. Immunol. Methods* 270: 183–197.

38. Williams, M. E., J. J. Densmore, A. W. Pawluczkowycz, P. V. Beum, A. D. Kennedy, M. A. Lindorfer, S. H. Hamil, J. C. Eggleton, and R. P. Taylor. 2006. Thrice-weekly low-dose rituximab decreases CD20 loss via shaving and promotes enhanced targeting in chronic lymphocytic leukemia. *J. Immunol.* 177: 7435–7443.

39. Taylor, R. P., A. W. Pawluczkowycz, P. V. Beum, M. A. Lindorfer, F. B. Beurskens, J. van de Winkel, and P. Parren. 2007. Complement activation and complemented-mediated killing of B cells promoted by anti-CD20 monoclonal antibodies (mAb) rituximab and ofatumumab are rapid, and ofatumumab kills cells more rapidly and with greater efficacy. *Blood* 118: 695a.

40. Cragg, M. S., C. A. Walshe, A. O. Ivanov, and M. J. Glennie. 2005. The biology of CD20 and its potential as a target for mAb therapy. *Curr. Dir. Autoimmun.* 8: 140–174.

41. Walport, M. J. 2001. Complement. *N. Engl. J. Med.* 344: 1058–1066.

42. Laine, R. O., B. P. Morgan, and A. F. Esser. 1988. Comparison between complement and melitting hemolysis: anti-melitting antibodies inhibit complement lysis. *Biochemistry* 27: 5308–5314.

43. Reiter, Y., A. Ciobotariu, J. Jones, B. P. Morgan, and Z. Fishelson. 1995. Complement membrane attack complex, perforin, and bacterial exotoxins induce in K562 cells calcium-dependent cross-protection from lysis. *J. Immunol.* 155: 2203–2210.

44. Loor, F., and L. B. Hagg. 1975. The modulation of microprojections on the lymphocyte membrane and the redistribution of membrane-bound ligands, a correlation. *Eur. J. Immunol.* 5: 854–865.

45. Morgan, B. P., J. R. Dankert, and A. F. Esser. 1987. Recovery of human neutrophils from complement attack: removal of the membrane attack complex by endocytosis and exocytosis. *J. Immunol.* 138: 246–253.

46. Pilzer, D., and Z. Fishelson. 2005. Mortalin/GRP75 promotes release of membrane vesicles from immune attacked cells and protection from complement-mediated lysis. *Int. Immunol.* 17: 1239–1248.

47. Pilzer, D., O. Gasser, O. Moskovich, J. A. Schifferli, and Z. Fishelson. 2005. Emission of membrane vesicles: roles in complement resistance, immunity and cancer. *Springer Semin. Immun.* 27: 375–387.

48. Moskovich, O., and Z. Fishelson. 2007. Live cell imaging of outward and inward vesiculation induced by the complement C5b-9 complex. *J. Biol. Chem.* 282: 29977–29986.

49. Gelderman, K. A., S. Tomlinson, G. D. Ross, and A. Gorter. 2004. Complement function in mAb-mediated cancer immunotherapy. *Trends Immunol.* 25: 158–164.

50. Treon, S., C. Mistsiades, N. Mistsiades, G. Young, D. Doss, R. Schlossman, and K. Anderson. 2001. Tumor cell expression of CD59 is associated with resistance to CD20 serotherapy in patients with B-cell malignancies. *J. Immunother.* 24: 263–271.

51. Gorter, A., and S. Meri. 1999. Immune evasion of tumor cells using membrane-bound complement regulatory proteins. *Immunol. Today* 20: 576–582.

52. Jurianz, K., S. Ziegler, H. Garcia-Schuler, S. Kraus, O. Bohana-Kashtan, Z. Fishelson, and M. Kirschfink. 1999. Complement resistance of tumor cells: basal and induced mechanisms. *Mol. Immunol.* 36: 929–939.

53. Macor, P., and F. Tedesco. 2007. Complement as effector system in cancer immunotherapy. *Immunol. Lett.* 111: 6–13.

54. van Dam, A. P., A. Oei, R. Jaspars, C. Fijen, B. Wilske, L. Spanjaard, and J. Dankert. 1997. Complement-mediated serum sensitivity among spirochetes that cause Lyme disease. *Infect. Immun.* 65: 1228–1236.

55. Toney, D. M., and F. Marciano-Cabral. 1994. Membrane vesiculation of *Naegleria flowleri* amoebae as a mechanism for resisting complement damage. *J. Immunol.* 152: 2952–2959.

56. Quigg, R. J., A. V. Cybulsky, J. B. Jacobs, and D. J. Salant. 1988. Anti-Fx1A prodcues complement-dependent cytotoxicity of glomerular epithelial cells. *Kidney Int.* 34: 43–52.

57. Mathas, S., A. Rickers, K. Bommert, B. Dorken, and M. Mapara. 2000. Anti-CD20-and B-cell receptor-mediated apoptosis: evidence for shared intracellular signaling pathways. *Cancer Res.* 60: 7170–7176.

58. Byrd, J. C., S. Kitada, I. W. Flinn, J. L. Aron, M. Pearson, D. Lucas, and J. C. Reed. 2002. The mechanism of tumor cell clearance by rituximab in vivo in patients with B-cell chronic lymphocytic leukemia: evidence of caspase activation and apoptosis induction. *Blood* 99: 1038–1043.

59. Shan, D., J. A. Ledbetter, and O. W. Press. 1998. Apoptosis of malignant human B cells by ligation of CD20 with monoclonal antibodies. *Blood* 91: 1644–1652.

60. Golay, J., M. Lazzari, V. Facchinetti, S. Bernasconi, G. Borleri, T. Barbui, A. Rambaldi, and M. Introna. 2001. CD20 levels determine the in vitro susceptibility to rituximab and complement of B-cell chronic lymphocytic leukemia: further regulation by CD55 and CD59. *Blood* 98: 3383–3389.

61. Werfel, T., M. Oppermann, M. Schulze, G. Krieger, M. Weber, and O. Gotze. 1992. Binding of fluorescein-labeled anaphylatoxin C5a to human peripheral blood, spleen, and bone marrow leukocytes. *Blood* 79: 152–160.

62. Nobes, C. D., and A. Hall. 1995. Rho, Rac, and Cdc42 GTPases regulate the assembly of multimolecular focal complexes associated with actin stress fibers, lamellipodia, and filopodia. *Cell* 81: 53–62.

63. Etienne-Manneville, S., and A. Hall. 2002. Rho GTPases in cell biology. *Nature* 420: 629–635.

64. Hall, A. 2005. Rho GTPases and the control of cell behaviour. *Biochem. Soc. Trans.* 33: 891–895.